
**Measurement of the cross section of high transverse
momentum $Z \rightarrow b\bar{b}$ production
in proton–proton collisions at $\sqrt{s} = 8$ TeV with the ATLAS
Detector**

The ATLAS Collaboration

Abstract

This Letter reports the observation of a high transverse momentum $Z \rightarrow b\bar{b}$ signal in proton–proton collisions at $\sqrt{s} = 8$ TeV and the measurement of its production cross section. The data analysed were collected in 2012 with the ATLAS detector at the LHC and correspond to an integrated luminosity of 19.5 fb^{-1} . The $Z \rightarrow b\bar{b}$ decay is reconstructed from a pair of b -tagged jets, clustered with the anti- k_t jet algorithm with $R = 0.4$, that have low angular separation and form a dijet with $p_T > 200$ GeV. The signal yield is extracted from a fit to the dijet invariant mass distribution, with the dominant, multi-jet background mass shape estimated by employing a fully data-driven technique that reduces the dependence of the analysis on simulation. The fiducial cross section is determined to be

$$\sigma_{Z \rightarrow b\bar{b}}^{\text{fid}} = 2.02 \pm 0.20 \text{ (stat.)} \pm 0.25 \text{ (syst.)} \pm 0.06 \text{ (lumi.) pb} = 2.02 \pm 0.33 \text{ pb},$$

in good agreement with next-to-leading-order theoretical predictions.

Measurement of the cross section of high transverse momentum $Z \rightarrow b\bar{b}$ production in proton–proton collisions at $\sqrt{s} = 8$ TeV with the ATLAS Detector

ATLAS Collaboration

Abstract

This Letter reports the observation of a high transverse momentum $Z \rightarrow b\bar{b}$ signal in proton–proton collisions at $\sqrt{s} = 8$ TeV and the measurement of its production cross section. The data analysed were collected in 2012 with the ATLAS detector at the LHC and correspond to an integrated luminosity of 19.5 fb^{-1} . The $Z \rightarrow b\bar{b}$ decay is reconstructed from a pair of b -tagged jets, clustered with the anti- k_t jet algorithm with $R = 0.4$, that have low angular separation and form a dijet with $p_T > 200$ GeV. The signal yield is extracted from a fit to the dijet invariant mass distribution, with the dominant, multi-jet background mass shape estimated by employing a fully data-driven technique that reduces the dependence of the analysis on simulation. The fiducial cross section is determined to be

$$\sigma_{Z \rightarrow b\bar{b}}^{\text{fid}} = 2.02 \pm 0.20 \text{ (stat.)} \pm 0.25 \text{ (syst.)} \pm 0.06 \text{ (lumi.) pb} = 2.02 \pm 0.33 \text{ pb},$$

in good agreement with next-to-leading-order theoretical predictions.

Keywords: LHC, boosted $b\bar{b}$ topologies

1. Introduction

High transverse momentum (p_T), hadronically decaying, electroweak-scale bosons have already been used in searches at the LHC [1–5], and are expected to play an increasingly significant role as the LHC moves to higher centre-of-mass energies in 2015. Therefore it is important to study them directly. This Letter presents the observation of a high- p_T $Z \rightarrow b\bar{b}$ signal in a fully hadronic final state, and a measurement of its production cross section. The measurement is compared to the next-to-leading-order (NLO) matrix element plus parton-shower predictions of POWHEG [6–9] and aMC@NLO [10], where the parton-shower, hadronisation and underlying-event modelling are provided by PYTHIA-8.165 [11] and HERWIG++ [12] respectively. This first measurement of a high- p_T electroweak-scale boson in an all-hadronic final state at the LHC demonstrates the validity of both the analysis techniques used and of the state-of-the-art NLO plus parton-shower particle-level predictions for electroweak-scale bosons decaying to $b\bar{b}$. It is therefore of great relevance for the search for the $H \rightarrow b\bar{b}$ signal in the (most sensitive) high Higgs boson p_T range [13], as well as for searches for TeV-scale resonances decaying to $b\bar{b}b\bar{b}$ via ZZ , ZH or HH [14, 15]. A high- p_T $Z \rightarrow b\bar{b}$ signal can also provide a useful benchmark for validating the performance of the ATLAS detector (for example, the b -jet energy scale¹); and for testing and optimising analysis methods relevant for physics studies involving high- p_T jets that contain b -hadrons (b -jets).

The analysis described in this Letter is designed to select $b\bar{b}$ decays of Z -bosons with $p_T > 200$ GeV, in proton–proton collisions

at $\sqrt{s} = 8$ TeV. The high- p_T requirement helps to enhance the signal relative to $b\bar{b}$ production in multi-jet events (predominantly gluon splitting to $b\bar{b}$ in this high- p_T regime), which is the dominant source of background and has a more steeply-falling p_T spectrum. In order to minimise the dependence on simulation, the analysis employs a fully data-driven technique for the determination of the invariant mass spectrum of the multi-jet background. This is especially important given that Monte Carlo (MC) generators have not been tested thoroughly in this region of the $b\bar{b}$ production phase space.

2. The ATLAS detector

ATLAS is a multi-purpose particle physics experiment [17] at the LHC. The detector layout² consists of inner tracking devices surrounded by a superconducting solenoid, electromagnetic and hadronic calorimeters, and a muon spectrometer. The inner tracking system provides charged-particle tracking in the pseudorapidity region $|\eta| < 2.5$ and vertex reconstruction. It consists of a silicon pixel detector, a silicon microstrip tracker, and a straw-tube transition radiation tracker. The system is surrounded by a solenoid that produces a 2 T axial magnetic field. The central calorimeter system consists of a liquid-argon electromagnetic (EM) sampling calorimeter with

¹The use of the $Z \rightarrow b\bar{b}$ peak to constrain the b -jet energy scale at the Tevatron experiments was demonstrated in Ref. [16].

²ATLAS uses a right-handed coordinate system with its origin at the nominal interaction point (IP) in the centre of the detector and the z -axis along the beam pipe. The x -axis points from the IP to the centre of the LHC ring, and the y -axis points upwards. Cylindrical coordinates (r, ϕ) are used in the transverse plane, ϕ is the azimuthal angle around the beam pipe. The pseudorapidity, η , is defined in terms of the polar angle θ as $\eta = -\ln[\tan(\theta/2)]$.

high granularity and an iron/scintillator-tile calorimeter providing hadronic energy measurements in the central pseudorapidity range ($|\eta| < 1.7$). The endcap and forward regions are instrumented with liquid-argon calorimeters for both electromagnetic and hadronic energy measurements up to $|\eta| = 4.9$. The muon spectrometer is operated in a magnetic field provided by air-core superconducting toroids and includes tracking chambers for precise muon momentum measurements up to $|\eta| = 2.7$ and trigger chambers covering the range $|\eta| < 2.4$. A three-level trigger system is used to select interesting events [18]. The Level-1 trigger reduces the event rate to below 75 kHz using hardware-based trigger algorithms acting on a subset of detector information. Two software-based trigger levels, referred to collectively as the High-Level Trigger (HLT), further reduce the event rate to about 400 Hz using information from the entire detector.

3. Data, simulated samples, and event reconstruction

The data sample used in this analysis, after requiring that certain quality criteria be satisfied, corresponds to an integrated luminosity of $\mathcal{L} = 19.5 \pm 0.5 \text{ fb}^{-1}$, and was recorded by ATLAS in 2012. The uncertainty on the integrated luminosity is derived, following the same methodology as that detailed in Ref. [19], from a calibration of the luminosity scale using beam-separation scans performed in November 2012.

MC event samples simulated with the GEANT4-based [20] ATLAS detector simulation [21] are used to model the $Z \rightarrow b\bar{b}$ signal and the small $t\bar{t}$, $Z \rightarrow c\bar{c}$ and $W \rightarrow q\bar{q}'$ background contributions. In addition, multi-jet MC event samples are used for studying the trigger modelling in simulation. The effect of multiple proton-proton interactions in the same bunch crossing (pile-up) is included in the simulation.

The $Z \rightarrow b\bar{b}$ signal is modelled using SHERPA-1.4.3 [22], with the CT10 [23] NLO parton distribution function (PDF) set. An alternative $Z \rightarrow b\bar{b}$ model was generated with PYTHIA-8.165 [11] and the CTEQ6L1 [24] leading-order (LO) PDF set and is used to determine the systematic uncertainty associated with $Z \rightarrow b\bar{b}$ modelling. The $Z \rightarrow c\bar{c}$ background is also generated with SHERPA-1.4.3 and the CT10 PDF set. The $t\bar{t}$ background is simulated with MC@NLO-4.06 [25] interfaced to HERWIG-6.520 [26] for the fragmentation and hadronisation processes, including JIMMY-4.31 [27] for the underlying-event description. The top quark mass is fixed at 172.5 GeV, and the PDF set CT10 is used. The $W \rightarrow q\bar{q}'$ and multi-jet MC samples are generated using PYTHIA-8.165 with the CT10 PDF set.

Jets are reconstructed using the anti- k_r jet clustering algorithm [28], with radius parameter $R = 0.4$. The inputs to the reconstruction algorithm are topological calorimeter cell clusters [29] calibrated at the EM energy scale. The effects of pile-up on jet energies are accounted for by a jet-area-based correction [30]. Jets are then calibrated to the hadronic energy scale using p_T - and η -dependent calibration factors based on MC simulations and the combination of several *in situ* techniques applied to data [29]. To remove jets with a significant contribution from pile-up interactions, it is required that at least

50% of the summed scalar p_T of tracks matched to a jet belongs to tracks originating from the primary vertex.³

The flavour of jets in the ATLAS simulation is defined by matching jets to hadrons with $p_T > 5 \text{ GeV}$. A jet is labelled as a b -jet if a b -hadron is found within $\Delta R = \sqrt{(\Delta\eta)^2 + (\Delta\phi)^2} = 0.3$ of the jet axis; otherwise, if a c -hadron is found within the same distance the jet is labeled as a c -jet; and if neither is the case then the jet is labelled as a light (quark) jet. The lifetime and other properties of b -hadrons are used to identify (b -tag) b -jets with $|\eta| < 2.5$, by exploiting the properties and topology of their decay products, such as the impact parameter of tracks (defined as a track's distance of closest approach to the primary vertex in the transverse plane), the presence of displaced vertices, and the reconstruction of c -hadron and b -hadron decays. The b -tagging algorithm used in this analysis [31] combines the above information using multivariate techniques and is configured to achieve an efficiency of 70% for tagging b -jets in a MC sample of $t\bar{t}$ events, while rejecting 80% of c -jets and more than 99% of light jets in the same sample.

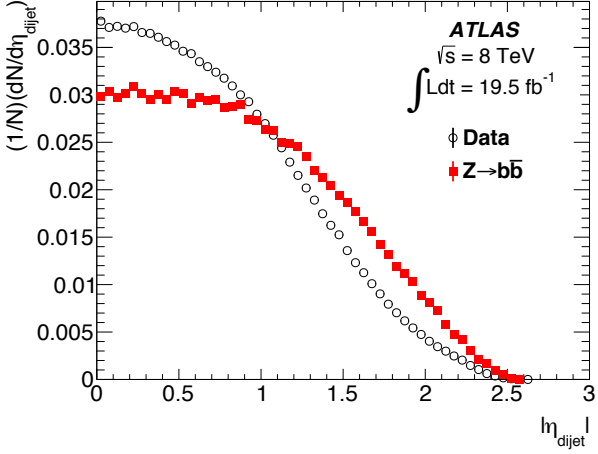
4. Event selection

The events of interest in this analysis were triggered by a combination of six jet-based triggers. The most efficient of these triggers (accepting about 70% of the signal events) requires two jets identified as b -jets by a dedicated HLT b -tagging algorithm, with transverse energies (E_T) above 35 GeV, and a jet with $E_T > 145 \text{ GeV}$ that may or may not be one of the b -tagged jets. The trigger efficiency for the SHERPA signal events passing the full offline event selection is 88.1%.

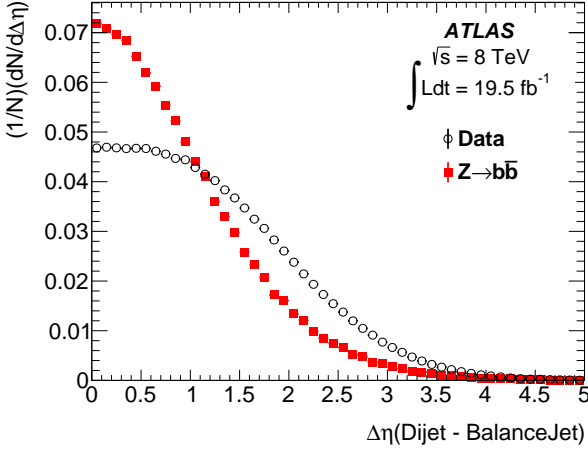
The event selection requires that there be at least three but no more than five jets with $|\eta| < 2.5$ and $p_T > 30 \text{ GeV}$, and that exactly two of them be b -tagged. The b -tagged jets must each have $p_T > 40 \text{ GeV}$. The angular distance, ΔR , between them must be smaller than 1.2 and the transverse momentum of the dijet system they form, p_T^{dijet} , must be greater than 200 GeV.

The final step of the event selection uses two variables with significant discrimination between signal and background to define two sets of events, one signal-enriched and the other signal-depleted, referred to hereafter as ‘‘Signal Region’’ and ‘‘Control Region’’. The two variables, which are combined with an artificial neural network (ANN) into a single discriminant, \mathcal{S}_{NN} , are: (1) the dijet pseudorapidity, η_{dijet} ; and (2) the pseudorapidity difference, $\Delta\eta$, between the dijet and the balancing jet, where the balancing jet is chosen to be the one that, when added to the dijet, gives the three-jet system with the smallest transverse momentum. The correlation of these two variables with the dijet invariant mass, m_{dijet} , is very small, allowing the ANN to be trained using selected data events outside the mass window [80, 110] GeV as background and $Z \rightarrow b\bar{b}$ MC events as signal. Fig. 1 depicts the distributions of η_{dijet} , $\Delta\eta$ and \mathcal{S}_{NN} in the signal MC sample and in the data. The data shown here include all events with $60 < m_{\text{dijet}} < 160 \text{ GeV}$, and are representative of the background as the signal contribution is estimated to

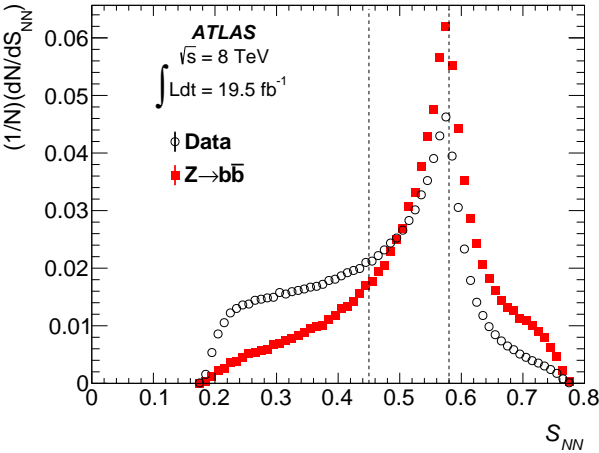
³Amongst all reconstructed proton-proton collisions in a bunch crossing, the primary vertex is defined as the vertex with the highest summed track p_T^2 .



(a)



(b)



(c)

Figure 1: The distributions of: (a) the dijet pseudorapidity, $|\eta_{\text{dijet}}|$; (b) the pseudorapidity difference, $|\Delta\eta|$, between the dijet and the balancing jet; and (c) the neural network discriminant S_{NN} , in the $Z \rightarrow b\bar{b}$ signal (red squares) and in the data (black circles), including all events with $60 < m_{\text{dijet}} < 160$ GeV. The data is dominated by the multi-jet background. The two dashed lines in (c) indicate the S_{NN} values defining the Signal ($S_{NN} > 0.58$) and Control ($S_{NN} < 0.45$) Regions.

be only about 1%. The Signal Region is defined by $S_{NN} > 0.58$ and the Control Region by $S_{NN} < 0.45$. The discriminating power of η_{dijet} and $\Delta\eta$ stems from the fact that signal production proceeds predominantly via a quark–gluon hard scatter, as opposed to the dominant multi-jet background which is largely initiated by gluon–gluon scattering. Due to the differences between the gluon and quark PDFs, the Z + jet system tends to be more boosted along the beam axis; hence the Z -boson is produced with higher η and smaller $\Delta\eta$ separation from its recoil, compared to the background.

Since S_{NN} is minimally correlated with m_{dijet} the Control Region can be used as an unbiased model of the background in the Signal Region. Fig. 2 shows the normalised ratio of the m_{dijet} distributions in the Signal and Control Regions, excluding the Z mass window. A first-order polynomial fit to this distribution gives a good χ^2 probability, 0.18, and a gradient consistent with zero, $(-1.37 \pm 1.10) \times 10^{-4} \text{ GeV}^{-1}$. In addition, the validity of assuming minimal correlation is supported by a test, performed with events from a PYTHIA 8 multi-jet MC sample satisfying the above analysis requirements, giving a ratio of the above distributions consistent with being flat. The impact of possible differences in the background m_{dijet} shape between the Signal and Control Regions is considered as one of the systematic uncertainties on the measurement.

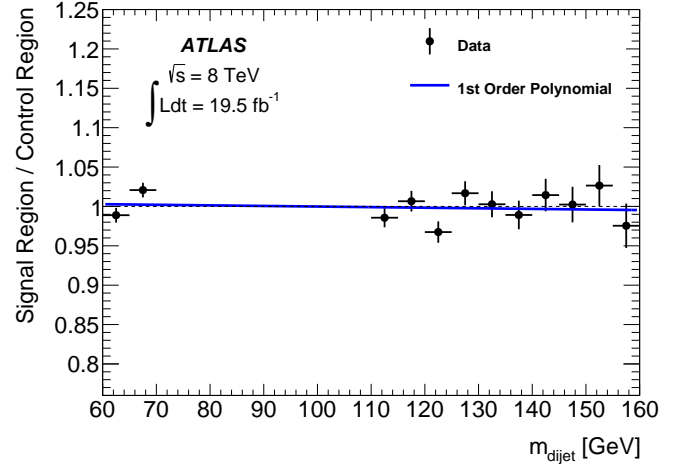


Figure 2: The normalised ratio of dijet mass distributions in the Signal and Control Regions, excluding the signal mass window, fitted with a first-order polynomial. The dashed line indicates unity.

The total number of data events satisfying the full analysis selection is 236172 in the Signal Region and 474810 in the Control Region. The signal-to-background ratio in a 30 GeV window around the Z -boson mass is expected to be about 6% (2%) in the Signal (Control) Region. The $t\bar{t}$ events are estimated to represent about 0.5% of the total background in both the Signal and Control Regions, and the $Z \rightarrow c\bar{c}$ and $W \rightarrow q\bar{q}'$ backgrounds are approximately 8% and 6% of the signal, respectively.

5. Cross-section definition

The fiducial cross section of resonant Z -boson production, with Z decaying to $b\bar{b}$, $\sigma_{Z\rightarrow b\bar{b}}^{\text{fid}}$, is defined as follows. Particle-level jets in MC $Z\rightarrow b\bar{b}$ events are reconstructed from stable particles (particles with lifetime in excess of 10 ps, excluding muons and neutrinos) using the anti- k_t algorithm with radius parameter $R = 0.4$. There must be two particle-level b -jets in the event that satisfy the following fiducial conditions: $p_T > 40$ GeV, $|\eta| < 2.5$ for the individual jets; and $\Delta R(\text{jet1}, \text{jet2}) < 1.2$, $p_T^{\text{dijet}} > 200$ GeV, $60 < m_{\text{dijet}} < 160$ GeV for the dijet system.

The cross section is extracted from the measured yield of $Z\rightarrow b\bar{b}$ events in the data, $N_{Z\rightarrow b\bar{b}}$, as

$$\sigma_{Z\rightarrow b\bar{b}}^{\text{fid}} = \frac{N_{Z\rightarrow b\bar{b}}}{\mathcal{L} \cdot C_{Z\rightarrow b\bar{b}}},$$

where $C_{Z\rightarrow b\bar{b}}$ is the efficiency correction factor to correct the detector-level $Z\rightarrow b\bar{b}$ yield to the particle level. The value of $C_{Z\rightarrow b\bar{b}}$ in the SHERPA MC signal is found to be 16.2%, which can be factorised into the product of: trigger efficiency (88.1%), b -tagging and kinematic selection efficiency (52.7%), and the efficiency of the \mathcal{S}_{NN} requirement that defines the Signal Region (35.0%). The uncertainties on $C_{Z\rightarrow b\bar{b}}$ are discussed in Section 7.

6. Signal extraction

The signal yield is extracted by fitting simultaneously the m_{dijet} distributions of the Signal and Control Regions in the range [60, 160] GeV with a binned, extended maximum-likelihood (EML) fit, using a bin width of 1 GeV.

The $Z\rightarrow b\bar{b}$ signal shape is modelled in the EML fit as the sum of three Gaussians. This empirical model describes well both the SHERPA and the PYTHIA signal MC samples, albeit with slightly different parameters. Given this, the SHERPA-based model is used as the baseline for the fit, and the PYTHIA-based model is used for an estimate of the systematic uncertainty on the measurement due to the signal shape. The only free parameters of the signal model in the EML fit are the yield in the Signal Region and the shift, δM_Z , of the mean of the narrowest Gaussian from its MC-predicted value. The widths and relative contributions of the three Gaussians, as well as the differences between the mean of each of the two wider Gaussians and the narrowest one, are fixed to the values determined by a separate fit to the signal MC m_{dijet} distributions. Given that the Control Region is not signal-free, the simultaneous fit includes a signal component in both the Signal Region and the Control Region. The relative proportion of signal in the two regions, $R_Z = (N_{Z\rightarrow b\bar{b}}^{\text{Control}})/(N_{Z\rightarrow b\bar{b}}^{\text{Signal}})$, is fixed to the value predicted by SHERPA, $R_Z = 0.62$. This choice is supported by the good agreement found between SHERPA and data in the \mathcal{S}_{NN} distribution obtained from a pure sample of high- p_T $Z\rightarrow \mu^+\mu^-$ events, as discussed in Section 7.

The dominant multi-jet background is modelled in the EML fit using a seventh-order Bernstein polynomial [32]. This is purely an empirical model and the order of the polynomial is

chosen by a χ^2 probability saturation test by fitting the m_{dijet} distribution in the Control Region with the background-only hypothesis and an increasing polynomial order, until no improvement is seen in the fit quality when adding higher-order terms. The coefficients of the Bernstein polynomial are determined by the simultaneous EML fit and are identical for the Signal and Control Regions. In this way, the signal-depleted Control Region constrains the background prediction in the Signal Region. The only additional parameters of the fit are the background normalisations in the Signal and Control Regions.

The small $Z\rightarrow c\bar{c}$, $t\bar{t}$ and $W\rightarrow q\bar{q}'$ backgrounds are included as separate components in the EML fit for both the Signal and Control Regions, with their m_{dijet} shapes being parameterised from MC simulation as follows. The $Z\rightarrow c\bar{c}$ and $W\rightarrow q\bar{q}'$ components are each modelled as three-Gaussian sums like the signal, with all parameters fixed to values from fits to MC simulation. The means of the Gaussians are expressed with respect to the mean of the narrowest $Z\rightarrow b\bar{b}$ Gaussian: this couples the position of these backgrounds to the $Z\rightarrow b\bar{b}$ signal. The $W\rightarrow q\bar{q}'$ component is normalised absolutely to its PYTHIA LO cross section, corrected to NLO by a K -factor derived using MCFM [33]. The acceptance of the $Z\rightarrow c\bar{c}$ background is taken from the simulation, but its yield is linked to the fitted $Z\rightarrow b\bar{b}$ yield, since the $Z\rightarrow c\bar{c}$ production differs from the signal only in the well-known branching fractions of the Z decays. All properties of the $t\bar{t}$ component are fixed using the $t\bar{t}$ simulation, with normalisation from the NNLO+NNLL prediction of the $t\bar{t}$ production cross section [34–39]. The contribution from Higgs decays to $b\bar{b}$ is expected to be $\sim 3\%$ of the $Z\rightarrow b\bar{b}$ signal and localised away from the signal peak: therefore no such component is included in the EML fit.

The fit procedure has been validated using a comprehensive set of tests based on pseudo-experiments, which have demonstrated that the yield and its uncertainty are accurately determined by the fit procedure over a wide range of input signal yields. In particular, the fit procedure is robust against fitting artefacts like false dips or peaks: a consequence of fitting both signal and control regions simultaneously, with the ratio of $Z\rightarrow b\bar{b}$ in each region fixed.

Fig. 3 shows the result of the simultaneous fit to the m_{dijet} distributions of the Signal and Control Regions, as well as the corresponding background-subtracted data distributions. The rather complex shape of the background invariant mass distribution results from the use of the six jet-based triggers, all of which have different jet p_T thresholds and hence shape differently the invariant mass distributions. The fitted function models the data well, with a signal peak compatible with $Z\rightarrow b\bar{b}$ decays. The fitted signal yield is 6420 ± 640 (stat.) events.

7. Systematic uncertainties

The sources of systematic uncertainties considered in this analysis, which may affect the fitted signal yield, the efficiency correction factor or both, are listed in Table 1.

The jet energy scale (JES) and jet energy resolution (JER) uncertainties are determined using the techniques described in

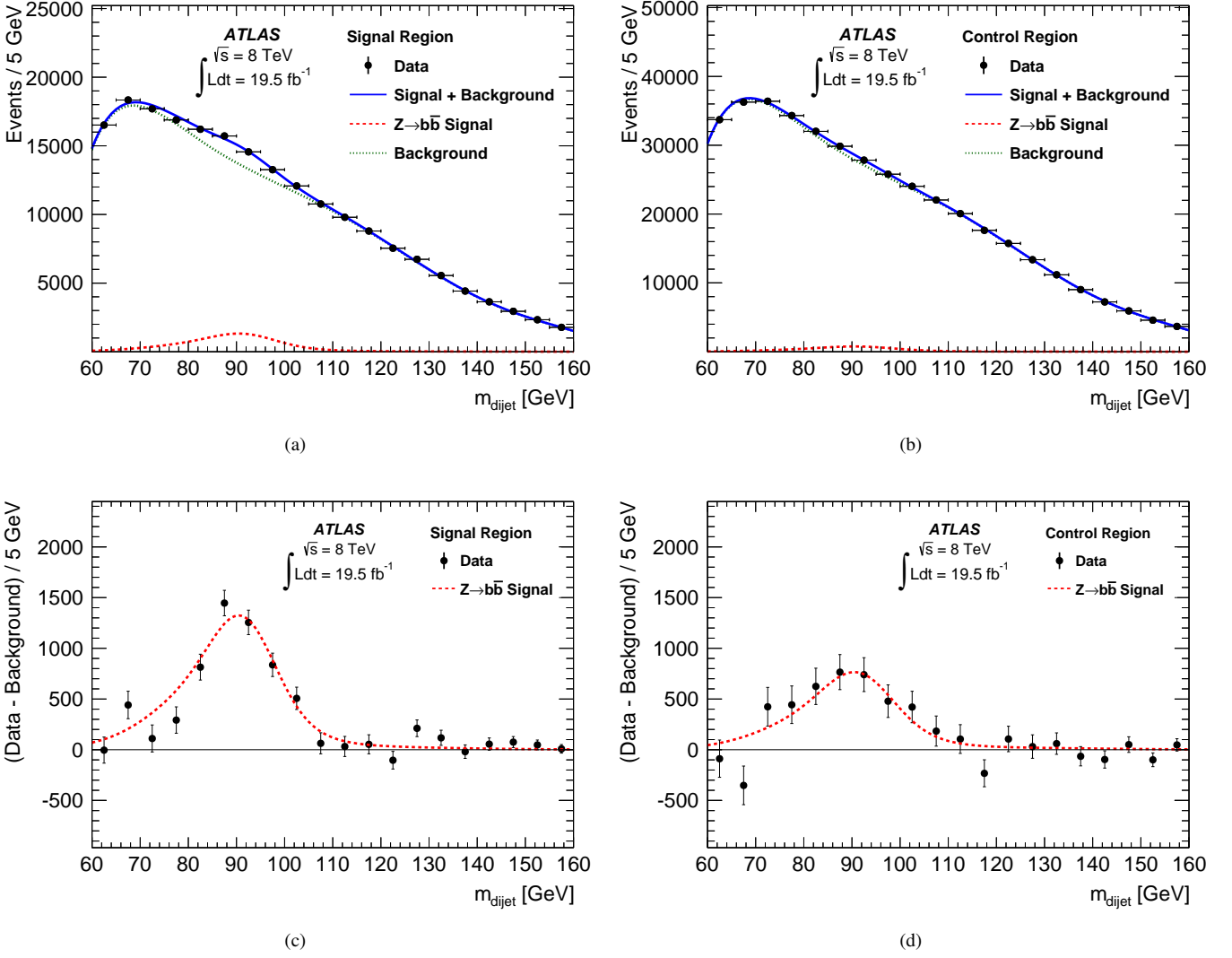


Figure 3: The result of the simultaneous extended maximum likelihood fit to the dijet mass distributions in (a) the Signal Region and (b) the Control Region, and the corresponding background-subtracted distributions (c) and (d), using the SHERPA signal model. The lines represent the signal (dashed), backgrounds (dotted) and the sum of the two (solid).

Refs. [29, 40]. The JES uncertainty has a relatively large impact on the signal efficiency, due to the p_T requirements on the individual jets and the dijet system, but a comparatively small impact on the fitted yield, because of the data-driven approach for the background determination and the fact that the location of the signal peak is a free parameter of the EML fit. The JER uncertainty affects predominantly the fitted yield, since it modifies the MC-derived signal shape.

The b -tagging efficiency in the simulation is scaled to reproduce the one in data and its uncertainty is evaluated by varying the data-to-MC scale factor applied to each jet in the simulation within a range that reflects the systematic uncertainty on the measured tagging efficiency for b -jets in ATLAS [31, 41]. The $Z \rightarrow c\bar{c}$ relative normalisation uncertainty is estimated in a similar way by varying the corresponding scale factors for charm jets in the simulation.

The uncertainty on $C_{Z \rightarrow b\bar{b}}$ due to a potential mis-modelling of the trigger efficiency is assessed using data events collected with a prescaled trigger that is fully efficient with respect to the analysis event selection. The full offline event selection is applied to these events and the efficiency for passing the analysis trigger requirements is compared to the corresponding efficiency in the multi-jet MC sample, as a function of various kinematic variables. It is found that the two trigger efficiencies are consistent to within 6%. Furthermore, the trigger efficiency in the multi-jet MC sample, when considering only those events where the two b -tagged jets are labelled as true b -jets, is fully consistent with the trigger efficiency in the signal MC events. Based on these studies, a $\pm 6\%$ trigger efficiency modelling uncertainty is propagated to the cross-section measurement.

The uncertainty on the extracted signal yield due to potential differences in the background m_{dijet} shape between the Sig-

Table 1: The relative systematic uncertainties on the fitted yield of $Z \rightarrow b\bar{b}$, $N_{Z \rightarrow b\bar{b}}$; the efficiency correction factor, $C_{Z \rightarrow b\bar{b}}$; and the fiducial cross-section, $\sigma_{Z \rightarrow b\bar{b}}^{\text{fid}}$, from each of the sources of uncertainty considered.

Source of uncertainty	$\Delta N_{Z \rightarrow b\bar{b}}(\%)$	$\Delta C_{Z \rightarrow b\bar{b}}(\%)$	$\Delta \sigma_{Z \rightarrow b\bar{b}}^{\text{fid}}(\%)$
Jet energy scale	+3.0/ - 1.5	± 8.4	+6.5/ - 5.0
Jet energy resolution	± 5.3	± 0.2	± 5.1
b -tagging	± 0.1	± 3.6	± 3.6
Trigger modelling	N/A	± 6	± 6
Control Region bias	+4.9/ - 5.5	N/A	+4.9/ - 5.5
Signal S_{NN} modelling	± 0.9	∓ 2.0	± 2.9
Signal m_{dijet} shape	± 2.2	N/A	± 2.2
$Z \rightarrow c\bar{c}$ normalisation	± 0.4	N/A	± 0.4
$t\bar{t}$ normalisation	± 1.2	N/A	± 1.1
$W \rightarrow q\bar{q}'$ normalisation	± 1.0	N/A	± 1.0

nal and Control Regions (“Control Region bias”) is assessed by repeating the EML fit for a range of S_{NN} values around the one used in the baseline selection to define the Control Region. These variations of the Control Region definition lead to small biases in the m_{dijet} shape relative to the Signal Region, resulting in non-zero slopes in the first-order polynomial fits to the distributions equivalent to the one in Fig. 2. The non-zero slopes of these fits bracket the statistical uncertainty with which the slope of the first-order polynomial fit to Fig. 2 is determined. The largest upwards and downwards variations in the fitted signal yield from the EML fits following this procedure are propagated as systematic uncertainty to the cross-section measurement.

The impact on $C_{Z \rightarrow b\bar{b}}$ of a possible mis-modelling of the distributions of the analysis selection variables, except S_{NN} , in the MC signal is assessed by comparing the SHERPA and PYTHIA MC signal samples. It is found to be less than 1% and therefore it is considered negligible. There is a 15% discrepancy between the PYTHIA and SHERPA predictions for the efficiency of the Signal Region S_{NN} requirement. Since the input variables to S_{NN} depend primarily on the dynamics of Z -boson production, the modelling by SHERPA is tested by comparing a sample of events in the ATLAS 2012 data containing high- p_T $Z \rightarrow \mu^+\mu^-$ decays to a corresponding SHERPA MC sample, with the dimuon system replacing the dijet system. The agreement is found to be very good, at the level of 2%, and the residual discrepancies are propagated as the “Signal S_{NN} modelling” uncertainty on both $C_{Z \rightarrow b\bar{b}}$ and the R_Z fit parameter. This uncertainty also covers the impact from possible differences between the PDFs used in the SHERPA signal sample and the data, given that the above $Z \rightarrow \mu^+\mu^-$ SHERPA sample uses the same PDF set as the $Z \rightarrow b\bar{b}$ SHERPA signal sample.

The difference obtained in the fitted signal yield when using the PYTHIA signal model rather than the SHERPA one is used as an estimate of the uncertainty on the measurement due to possible mis-modelling of the m_{dijet} shape in the MC signal.

The impact on the measurement from the uncertainty on the $W \rightarrow q\bar{q}'$ and $t\bar{t}$ normalisations is assessed by varying the fixed number of events of each background in the Signal and Control

Regions independently by 50% and repeating the EML fit.

8. Results

Using the extracted $Z \rightarrow b\bar{b}$ yield, the estimated signal-efficiency correction factor and the integrated luminosity of the dataset, the cross section in the fiducial region defined in Section 5 is measured to be

$$\sigma_{Z \rightarrow b\bar{b}}^{\text{fid}} = 2.02 \pm 0.20 (\text{stat.}) \pm 0.25 (\text{syst.}) \pm 0.06 (\text{lumi.}) \text{ pb}.$$

The total systematic uncertainty is the result of adding in quadrature all the individual systematic uncertainties on $\sigma_{Z \rightarrow b\bar{b}}^{\text{fid}}$ listed in Table 1. It is further found that the signal m_{dijet} peak position is consistent with the $Z \rightarrow b\bar{b}$ expectation: $\delta M_Z = -1.5 \pm 0.7 (\text{stat.})_{-2.5}^{+3.4} (\text{syst.}) \text{ GeV}$. The good agreement with zero provides an independent confirmation of the good agreement between data and MC on the energy scale of b -jets in ATLAS.

The robustness of the measurement is supported by several cross-checks and complementary studies. In particular, a consistent cross-section measurement is obtained by applying a tighter b -tagging selection (with an efficiency of 60% for tagging b -jets in a MC sample of $t\bar{t}$ events) or when the requirement on p_T^{dijet} is raised to 250 GeV or 300 GeV. Furthermore, when the same methodology is repeated on two independent classes of events, those accepted by the dominant trigger described above and all other events, both measured cross sections ($1.99 \pm 0.25 (\text{stat.}) \text{ pb}$ and $1.87 \pm 0.44 (\text{stat.}) \text{ pb}$ respectively) are fully consistent with the baseline measurement, even though the m_{dijet} distributions are significantly different in the two classes of events. In addition, when the background shape obtained from the baseline EML fit is used to fit for a signal in the sample of events with $0.45 < S_{NN} < 0.58$, the fitted signal yield in this sample is consistent with the number of signal events calculated based on the measured cross section and the shape of S_{NN} predicted by SHERPA. Finally, repeating the analysis with

a number of alternative functional forms for the empirical description of the background shape (such as a log-normal function convolved with a fourth-order Bernstein polynomial) leads to negligible variations in the measured cross section compared to the systematic uncertainties of the measurement.

The measured cross section is compared to the particle-level, NLO-plus-parton-shower predictions of two MC generators, POWHEG and aMC@NLO, in the same fiducial region. In both cases, the cross section of the $Z + 1$ -jet process is calculated to NLO accuracy. For aMC@NLO, the Z decay is simulated with MadSpin [42]. POWHEG is interfaced to PYTHIA for parton showering, hadronisation and underlying-event contributions, whilst aMC@NLO is interfaced to HERWIG++. The particle-level predictions are then derived by applying to the generated events the fiducial selection defined in Section 5. The predicted cross sections are:

$$\text{POWHEG} : \sigma_{Z \rightarrow b\bar{b}}^{\text{fid}} = 2.02^{+0.25}_{-0.19}(\text{scales})^{+0.03}_{-0.04}(\text{PDF}) \text{ pb}$$

$$\text{aMC@NLO} : \sigma_{Z \rightarrow b\bar{b}}^{\text{fid}} = 1.98^{+0.16}_{-0.08}(\text{scales}) \pm 0.03(\text{PDF}) \text{ pb}.$$

Both generators use the CT10 PDF set for the central value of the prediction, and the renormalisation and factorisation scales are set to the p_T of the Z boson. The uncertainty due to the ambiguity in the renormalisation and factorisation scales is estimated by doubling or halving them simultaneously. The PDF uncertainty is evaluated by varying the 52 PDFs in the CT10 NLO error set, following the Hessian method and rescaling to the 68% confidence level. Within the experimental and theoretical uncertainties, both predictions are completely consistent with the measured cross section.

POWHEG and aMC@NLO can also be used to provide an estimate of the fraction of the total cross section for $Z \rightarrow b\bar{b}$ production at the LHC, with $p_T > 200$ GeV, that is contained within the measured fiducial region. The ratio of the above cross sections to the cross sections calculated without applying any particle-level requirements, only requiring $p_T > 200$ GeV for the Z -boson before parton showering, is 0.53 for POWHEG and 0.47 for aMC@NLO.

In conclusion, the high- p_T $Z \rightarrow b\bar{b}$ signal has been observed and its production cross section measured in a fully hadronic final state, in 19.5 fb^{-1} of proton–proton collisions at $\sqrt{s} = 8$ TeV recorded in 2012 by the ATLAS detector at the LHC. Within the fiducial region defined in Section 5, the production cross section is measured to be

$$\sigma_{Z \rightarrow b\bar{b}}^{\text{fid}} = 2.02 \pm 0.20(\text{stat.}) \pm 0.25(\text{syst.}) \pm 0.06(\text{lumi.}) \text{ pb}$$

and is found to be in good agreement with the NLO-plus-parton-shower predictions from POWHEG and aMC@NLO.

Acknowledgements

We thank CERN for the very successful operation of the LHC, as well as the support staff from our institutions without whom ATLAS could not be operated efficiently.

We acknowledge the support of ANPCyT, Argentina; YerPhI, Armenia; ARC, Australia; BMWF and FWF, Austria;

ANAS, Azerbaijan; SSTC, Belarus; CNPq and FAPESP, Brazil; NSERC, NRC and CFI, Canada; CERN; CONICYT, Chile; CAS, MOST and NSFC, China; COLCIENCIAS, Colombia; MSMT CR, MPO CR and VSC CR, Czech Republic; DNRF, DNSRC and Lundbeck Foundation, Denmark; EPLANET, ERC and NSRF, European Union; IN2P3-CNRS, CEA-DSM/IRFU, France; GNSF, Georgia; BMBF, DFG, HGF, MPG and AvH Foundation, Germany; GSRT and NSRF, Greece; ISF, MINERVA, GIF, I-CORE and Benoziyo Center, Israel; INFN, Italy; MEXT and JSPS, Japan; CNRST, Morocco; FOM and NWO, Netherlands; BRF and RCN, Norway; MNiSW and NCN, Poland; GRICES and FCT, Portugal; MNE/IFA, Romania; MES of Russia and ROSATOM, Russian Federation; JINR; MSTD, Serbia; MSSR, Slovakia; ARRS and MIZŠ, Slovenia; DST/NRF, South Africa; MINECO, Spain; SRC and Wallenberg Foundation, Sweden; SER, SNSF and Cantons of Bern and Geneva, Switzerland; NSC, Taiwan; TAEK, Turkey; STFC, the Royal Society and Leverhulme Trust, United Kingdom; DOE and NSF, United States of America.

The crucial computing support from all WLCG partners is acknowledged gratefully, in particular from CERN and the ATLAS Tier-1 facilities at TRIUMF (Canada), NDGF (Denmark, Norway, Sweden), CC-IN2P3 (France), KIT/GridKA (Germany), INFN-CNAF (Italy), NL-T1 (Netherlands), PIC (Spain), ASGC (Taiwan), RAL (UK) and BNL (USA) and in the Tier-2 facilities worldwide.

References

- [1] ATLAS Collaboration, *Search for resonant diboson production in the $lvjj$ decay channels with the ATLAS detector at 7 TeV*, Phys. Rev. **D87** (2013) 112006, arXiv:1305.0125 [hep-ex].
- [2] CMS Collaboration, *Search for massive resonances in dijet systems containing jets tagged as W or Z boson decays in pp collisions at $\sqrt{s} = 8$ TeV*, Journal of High Energy Physics **2014** no. 8, (2014), arXiv:1405.1994.
- [3] CMS Collaboration, *Search for massive resonances decaying into pairs of boosted bosons in semi-leptonic final states at $\sqrt{s} = 8$ TeV*, Journal of High Energy Physics **2014** no. 8, (2014), arXiv:1405.3447.
- [4] ATLAS Collaboration, *Search for the Standard Model Higgs boson produced in association with a vector boson and decaying to a b -quark pair with the ATLAS detector*, Physics Letters B **718** no. 2, (2012) 369 – 390, arXiv:1207.0210.
- [5] *Search for the standard model Higgs boson decaying to bottom quarks in pp collisions at $\sqrt{s} = 7$ TeV*, Physics Letters B **710** no. 2, (2012) 284 – 306, arXiv:1202.4195.
- [6] S. Alioli, P. Nason, C. Oleari, and E. Re, *Vector boson plus one jet production in POWHEG*, JHEP **1101** (2011) 095, arXiv:1009.5594 [hep-ph]. Extended to include the $Z \rightarrow b\bar{b}$ decay by the authors.
- [7] P. Nason, *A new method for combining NLO QCD with shower Monte Carlo algorithms*, JHEP **0411** (2004) 040, arXiv:hep-ph/0409146 [hep-ph].
- [8] S. Frixione, P. Nason, and C. Oleari, *Matching NLO QCD computations with parton shower simulations: the POWHEG method*, JHEP **0711** (2007) 070, arXiv:0709.2092 [hep-ph].
- [9] S. Alioli, P. Nason, C. Oleari, and E. Re, *A general framework for implementing NLO calculations in shower Monte Carlo programs: the POWHEG BOX*, JHEP **1006** (2010) 043, arXiv:1002.2581 [hep-ph].
- [10] R. Frederix et al., *Scalar and pseudoscalar Higgs production in association with a top-antitop pair*, Phys. Lett. **B701** (2011) 427–433, arXiv:1104.5613 [hep-ph].

- [11] T. Sjostrand, S. Mrenna, and P. Z. Skands, *A Brief Introduction to PYTHIA 8.1*, Comput. Phys. Commun. **178** (2008) 852–867, arXiv:0710.3820 [hep-ph].
- [12] M. Bähr et al., *Herwig++ Physics and Manual*, Eur. Phys. J. **C58** (2008) 639–707, arXiv:0803.0883 [hep-ph].
- [13] ATLAS Collaboration, *Search for the Standard Model Higgs boson produced in association with a vector boson and decaying to a b-quark pair with the ATLAS detector*, Phys. Lett. **B718** (2012) 369–390, arXiv:1207.0210 [hep-ex].
- [14] B. Cooper, N. Konstantinidis, L. Lambourne, and D. Wardrope, *Boosted $hh \rightarrow bbbb$: A new topology in searches for TeV-scale resonances at the LHC*, Phys. Rev. D **88** (2013) 114005, arXiv:1307.0407 [hep-ex].
- [15] M. Gouzevitch et al., *Scale-invariant resonance tagging in multijet events and new physics in Higgs pair production*, JHEP **1307** (2013) 148, arXiv:1303.6636 [hep-ph].
- [16] J. Donini et al., *Energy calibration of b-quark jets with $Z \rightarrow b\bar{b}$ decays at the Tevatron collider*, Nucl. Instrum. Meth. **A596** (2008) 354–367, arXiv:0801.3906 [hep-ex].
- [17] ATLAS Collaboration, *The ATLAS experiment at the CERN Large Hadron Collider*, JINST **3** (2008) S08003.
- [18] ATLAS Collaboration, *Performance of the ATLAS trigger system in 2010*, Eur. Phys. J. **C72** (2012) 1849, arXiv:1110.1530 [hep-ex].
- [19] ATLAS Collaboration, *Improved luminosity determination in pp collisions at $\sqrt{s} = 7$ TeV using the ATLAS detector at the LHC*, Eur. Phys. J. **C73** (2013) 2518, arXiv:1302.4393 [hep-ex].
- [20] S. Agostinelli et al., *GEANT4 – a simulation toolkit*, Nucl. Instrum. Meth. **A506** (2003) 250.
- [21] ATLAS Collaboration, *The ATLAS simulation infrastructure*, Eur. Phys. J. **C70** (2010) 823–874, arXiv:1005.4568 [hep-ex].
- [22] T. Gleisberg et al., *Event generation with SHERPA 1.1*, JHEP **0902** (2009) 007, arXiv:0811.4622 [hep-ph].
- [23] H.-L. Lai et al., *New parton distributions for collider physics*, Phys. Rev. **D82** (2010) 074024, arXiv:1007.2241 [hep-ph].
- [24] J. Pumplin et al., *New generation of parton distributions with uncertainties from global QCD analysis*, JHEP **0207** (2002) 012, arXiv:hep-ph/0201195 [hep-ph].
- [25] S. Frixione and B. R. Webber, *Matching NLO QCD computations and parton shower simulations*, JHEP **0206** (2002) 029, arXiv:hep-ph/0204244 [hep-ph].
- [26] G. Corcella et al., *HERWIG 6.5: an event generator for hadron emission reactions with interfering gluons (including supersymmetric processes)*, JHEP **0101** (2001) 010, arXiv:hep-ph/0011363 [hep-ph].
- [27] J. Butterworth, J. R. Forshaw, and M. Seymour, *Multiparton interactions in photoproduction at HERA*, Z. Phys. **C72** (1996) 637–646, arXiv:hep-ph/9601371 [hep-ph].
- [28] M. Cacciari, G. P. Salam, and G. Soyez, *The anti- k_t jet clustering algorithm*, JHEP **0804** (2008) 063, arXiv:0802.1189 [hep-ph].
- [29] ATLAS Collaboration, *Jet energy measurement with the ATLAS detector in proton-proton collisions at $\sqrt{s} = 7$ TeV*, Eur. Phys. J. **C73** (2013) 2304, arXiv:1112.6426 [hep-ex].
- [30] M. Cacciari, G. P. Salam, and G. Soyez, *The catchment area of jets*, JHEP **0804** (2008) 005, arXiv:0802.1188 [hep-ph].
- [31] ATLAS Collaboration, *Measuring the b-tag efficiency in a top-pair sample with 4.7 fb^{-1} of data from the ATLAS detector*, ATLAS-CONF-2012-097, <http://cds.cern.ch/record/1460443>.
- [32] S. Bernstein, *Démonstration du théoreme de Weierstrass fondée sur le calcul des probabilités*, Comm. Soc. Math. Kharkov **13** (1912).
- [33] J. M. Campbell and R. Ellis, *MCFM for the Tevatron and the LHC*, Nucl. Phys. Proc. Suppl. **205-206** (2010) 10–15, arXiv:1007.3492 [hep-ph].
- [34] M. Cacciari et al., *Top-pair production at hadron colliders with next-to-next-to-leading logarithmic soft-gluon resummation*, Phys. Lett. **B710** (2012) 612–622, arXiv:1111.5869 [hep-ph].
- [35] P. Bärnreuther, M. Czakon, and A. Mitov, *Percent-level-precision physics at the Tevatron: first genuine NNLO QCD corrections to $q\bar{q} \rightarrow t\bar{t} + X$* , Phys. Rev. Lett. **109** (2012) 132001, arXiv:1204.5201 [hep-ph].
- [36] M. Czakon and A. Mitov, *NNLO corrections to top-pair production at hadron colliders: the all-fermionic scattering channels*, JHEP **1212** (2012) 054, arXiv:1207.0236 [hep-ph].
- [37] M. Czakon and A. Mitov, *NNLO corrections to top pair production at hadron colliders: the quark-gluon reaction*, JHEP **1301** (2013) 080, arXiv:1210.6832 [hep-ph].
- [38] M. Czakon, P. Fiedler, and A. Mitov, *The total top quark pair production cross-section at hadron colliders through $O(\alpha_s^4)$* , Phys. Rev. Lett. **110** (2013) 252004, arXiv:1303.6254 [hep-ph].
- [39] M. Czakon and A. Mitov, *Top++: a program for the calculation of the top-pair cross-section at hadron colliders*, arXiv:1112.5675 [hep-ph].
- [40] ATLAS Collaboration, *Jet energy resolution in proton-proton collisions at $\sqrt{s} = 7$ TeV recorded in 2010 with the ATLAS detector*, Eur. Phys. J. **C73** (2013) 2306, arXiv:1210.6210 [hep-ex].
- [41] ATLAS Collaboration, *Calibration of b-tagging using dileptonic top pair events in a combinatorial likelihood approach with the ATLAS experiment*, ATLAS-CONF-2014-004, <https://cds.cern.ch/record/1664335>.
- [42] J. Alwall et al., *MadGraph 5: going beyond*, JHEP **1106** (2011) 128, arXiv:1106.0522 [hep-ph].

M. Vreeswijk¹⁰⁶, T. Vu Anh⁴⁸, R. Vuillermet³⁰, I. Vukotic³¹, Z. Vykydal¹²⁷, W. Wagner¹⁷⁶, P. Wagner²¹, H. Wahlberg⁷⁰, S. Wahrmund⁴⁴, J. Wakabayashi¹⁰², J. Walder⁷¹, R. Walker⁹⁹, W. Walkowiak¹⁴², R. Wall¹⁷⁷, P. Waller⁷³, B. Walsh¹⁷⁷, C. Wang^{152,ah}, C. Wang⁴⁵, F. Wang¹⁷⁴, H. Wang¹⁵, H. Wang⁴⁰, J. Wang⁴², J. Wang^{33a}, K. Wang⁸⁶, R. Wang¹⁰⁴, S.M. Wang¹⁵², T. Wang²¹, X. Wang¹⁷⁷, C. Wanotayaroj¹¹⁵, A. Warburton⁸⁶, C.P. Ward²⁸, D.R. Wardrope⁷⁷, M. Warsinsky⁴⁸, A. Washbrook⁴⁶, C. Wasicki⁴², I. Watanabe⁶⁶, P.M. Watkins¹⁸, A.T. Watson¹⁸, I.J. Watson¹⁵¹, M.F. Watson¹⁸, G. Watts¹³⁹, S. Watts⁸³, B.M. Waugh⁷⁷, S. Webb⁸³, M.S. Weber¹⁷, S.W. Weber¹⁷⁵, J.S. Webster³¹, A.R. Weidberg¹¹⁹, P. Weigell¹⁰⁰, B. Weinert⁶⁰, J. Weingarten⁵⁴, C. Weiser⁴⁸, H. Weits¹⁰⁶, P.S. Wells³⁰, T. Wenaus²⁵, D. Wendland¹⁶, Z. Weng^{152,ac}, T. Wengler³⁰, S. Wenig³⁰, N. Wermes²¹, M. Werner⁴⁸, P. Werner³⁰, M. Wessels^{58a}, J. Wetter¹⁶², K. Whalen²⁹, A. White⁸, M.J. White¹, R. White^{32b}, S. White^{123a,123b}, D. Whiteson¹⁶⁴, D. Wicke¹⁷⁶, F.J. Wickens¹³⁰, W. Wiedenmann¹⁷⁴, M. Wielers¹³⁰, P. Wienemann²¹, C. Wiglesworth³⁶, L.A.M. Wiik-Fuchs²¹, P.A. Wijeratne⁷⁷, A. Wildauer¹⁰⁰, M.A. Wildt^{42,ai}, H.G. Wilkens³⁰, J.Z. Will⁹⁹, H.H. Williams¹²¹, S. Williams²⁸, C. Willis⁸⁹, S. Willocq⁸⁵, J.A. Wilson¹⁸, A. Wilson⁸⁸, I. Wingerter-Seez⁵, F. Winklmeier¹¹⁵, B.T. Winter²¹, M. Wittgen¹⁴⁴, T. Wittig⁴³, J. Wittkowski⁹⁹, S.J. Wollstadt⁸², M.W. Wolter³⁹, H. Wolters^{125a,125c}, B.K. Wosiek³⁹, J. Wotschack³⁰, M.J. Woudstra⁸³, K.W. Wozniak³⁹, M. Wright⁵³, M. Wu⁵⁵, S.L. Wu¹⁷⁴, X. Wu⁴⁹, Y. Wu⁸⁸, E. Wulf³⁵, T.R. Wyatt⁸³, B.M. Wynne⁴⁶, S. Xella³⁶, M. Xiao¹³⁷, D. Xu^{33a}, L. Xu^{33b,aj}, B. Yabsley¹⁵¹, S. Yacoob^{146b,ak}, M. Yamada⁶⁵, H. Yamaguchi¹⁵⁶, Y. Yamaguchi¹⁵⁶, A. Yamamoto⁶⁵, K. Yamamoto⁶³, S. Yamamoto¹⁵⁶, T. Yamamura¹⁵⁶, T. Yamanaka¹⁵⁶, K. Yamauchi¹⁰², Y. Yamazaki⁶⁶, Z. Yan²², H. Yang^{33e}, H. Yang¹⁷⁴, U.K. Yang⁸³, Y. Yang¹¹⁰, S. Yanush⁹², L. Yao^{33a}, W-M. Yao¹⁵, Y. Yasu⁶⁵, E. Yatsenko⁴², K.H. Yau Wong²¹, J. Ye⁴⁰, S. Ye²⁵, A.L. Yen⁵⁷, E. Yildirim⁴², M. Yilmaz^{4b}, R. Yoosoofmiya¹²⁴, K. Yorita¹⁷², R. Yoshida⁶, K. Yoshihara¹⁵⁶, C. Young¹⁴⁴, C.J.S. Young³⁰, S. Youssef²², D.R. Yu¹⁵, J. Yu⁸, J.M. Yu⁸⁸, J. Yu¹¹³, L. Yuan⁶⁶, A. Yurkewicz¹⁰⁷, B. Zabinski³⁹, R. Zaidan⁶², A.M. Zaitsev^{129,y}, A. Zaman¹⁴⁹, S. Zambito²³, L. Zanello^{133a,133b}, D. Zanzi¹⁰⁰, C. Zeitnitz¹⁷⁶, M. Zeman¹²⁷, A. Zemla^{38a}, K. Zengel²³, O. Zenin¹²⁹, T. Ženiš^{145a}, D. Zerwas¹¹⁶, G. Zevi della Porta⁵⁷, D. Zhang⁸⁸, F. Zhang¹⁷⁴, H. Zhang⁸⁹, J. Zhang⁶, L. Zhang¹⁵², X. Zhang^{33d}, Z. Zhang¹¹⁶, Z. Zhao^{33b}, A. Zhemchugov⁶⁴, J. Zhong¹¹⁹, B. Zhou⁸⁸, L. Zhou³⁵, N. Zhou¹⁶⁴, C.G. Zhu^{33d}, H. Zhu^{33a}, J. Zhu⁸⁸, Y. Zhu^{33b}, X. Zhuang^{33a}, K. Zhukov⁹⁵, A. Zibell¹⁷⁵, D. Zieminska⁶⁰, N.I. Zimine⁶⁴, C. Zimmermann⁸², R. Zimmermann²¹, S. Zimmermann²¹, S. Zimmermann⁴⁸, Z. Zinonos⁵⁴, M. Ziolkowski¹⁴², G. Zobernig¹⁷⁴, A. Zoccoli^{20a,20b}, M. zur Nedden¹⁶, G. Zurzolo^{103a,103b}, V. Zutshi¹⁰⁷, L. Zwalinski³⁰.

¹ Department of Physics, University of Adelaide, Adelaide, Australia

² Physics Department, SUNY Albany, Albany NY, United States of America

³ Department of Physics, University of Alberta, Edmonton AB, Canada

⁴ (a) Department of Physics, Ankara University, Ankara; (b) Department of Physics, Gazi University, Ankara; (c) Division of Physics, TOBB University of Economics and Technology, Ankara; (d) Turkish Atomic Energy Authority, Ankara, Turkey

⁵ LAPP, CNRS/IN2P3 and Université de Savoie, Annecy-le-Vieux, France

⁶ High Energy Physics Division, Argonne National Laboratory, Argonne IL, United States of America

⁷ Department of Physics, University of Arizona, Tucson AZ, United States of America

⁸ Department of Physics, The University of Texas at Arlington, Arlington TX, United States of America

⁹ Physics Department, University of Athens, Athens, Greece

¹⁰ Physics Department, National Technical University of Athens, Zografou, Greece

¹¹ Institute of Physics, Azerbaijan Academy of Sciences, Baku, Azerbaijan

¹² Institut de Física d'Altes Energies and Departament de Física de la Universitat Autònoma de Barcelona, Barcelona, Spain

¹³ (a) Institute of Physics, University of Belgrade, Belgrade; (b) Vinca Institute of Nuclear Sciences, University of Belgrade, Belgrade, Serbia

¹⁴ Department for Physics and Technology, University of Bergen, Bergen, Norway

¹⁵ Physics Division, Lawrence Berkeley National Laboratory and University of California, Berkeley CA, United States of America

¹⁶ Department of Physics, Humboldt University, Berlin, Germany

¹⁷ Albert Einstein Center for Fundamental Physics and Laboratory for High Energy Physics, University of Bern, Bern, Switzerland

¹⁸ School of Physics and Astronomy, University of Birmingham, Birmingham, United Kingdom

¹⁹ (a) Department of Physics, Bogazici University, Istanbul; (b) Department of Physics, Dogus University, Istanbul; (c) Department of Physics Engineering, Gaziantep University, Gaziantep, Turkey

²⁰ (a) INFN Sezione di Bologna; (b) Dipartimento di Fisica e Astronomia, Università di Bologna, Bologna, Italy

²¹ Physikalisches Institut, University of Bonn, Bonn, Germany

²² Department of Physics, Boston University, Boston MA, United States of America

²³ Department of Physics, Brandeis University, Waltham MA, United States of America

²⁴ (a) Universidade Federal do Rio De Janeiro COPPE/EE/IF, Rio de Janeiro; (b) Federal University of Juiz de Fora (UFJF), Juiz de Fora; (c) Federal University of Sao Joao del Rei (UFSJ), Sao Joao del Rei; (d) Instituto de Fisica, Universidade de Sao Paulo, Sao Paulo, Brazil

²⁵ Physics Department, Brookhaven National Laboratory, Upton NY, United States of America

²⁶ (a) National Institute of Physics and Nuclear Engineering, Bucharest; (b) National Institute for Research and Development of Isotopic and Molecular Technologies, Physics Department, Cluj Napoca; (c) University Politehnica Bucharest, Bucharest; (d) West

University in Timisoara, Timisoara, Romania

²⁷ Departamento de Física, Universidad de Buenos Aires, Buenos Aires, Argentina

²⁸ Cavendish Laboratory, University of Cambridge, Cambridge, United Kingdom

²⁹ Department of Physics, Carleton University, Ottawa ON, Canada

³⁰ CERN, Geneva, Switzerland

³¹ Enrico Fermi Institute, University of Chicago, Chicago IL, United States of America

³² ^(a) Departamento de Física, Pontificia Universidad Católica de Chile, Santiago; ^(b) Departamento de Física, Universidad Técnica Federico Santa María, Valparaíso, Chile

³³ ^(a) Institute of High Energy Physics, Chinese Academy of Sciences, Beijing; ^(b) Department of Modern Physics, University of Science and Technology of China, Anhui; ^(c) Department of Physics, Nanjing University, Jiangsu; ^(d) School of Physics, Shandong University, Shandong; ^(e) Physics Department, Shanghai Jiao Tong University, Shanghai, China

³⁴ Laboratoire de Physique Corpusculaire, Clermont Université and Université Blaise Pascal and CNRS/IN2P3, Clermont-Ferrand, France

³⁵ Nevis Laboratory, Columbia University, Irvington NY, United States of America

³⁶ Niels Bohr Institute, University of Copenhagen, Kobenhavn, Denmark

³⁷ ^(a) INFN Gruppo Collegato di Cosenza, Laboratori Nazionali di Frascati; ^(b) Dipartimento di Fisica, Università della Calabria, Rende, Italy

³⁸ ^(a) AGH University of Science and Technology, Faculty of Physics and Applied Computer Science, Krakow; ^(b) Marian Smoluchowski Institute of Physics, Jagiellonian University, Krakow, Poland

³⁹ The Henryk Niewodniczanski Institute of Nuclear Physics, Polish Academy of Sciences, Krakow, Poland

⁴⁰ Physics Department, Southern Methodist University, Dallas TX, United States of America

⁴¹ Physics Department, University of Texas at Dallas, Richardson TX, United States of America

⁴² DESY, Hamburg and Zeuthen, Germany

⁴³ Institut für Experimentelle Physik IV, Technische Universität Dortmund, Dortmund, Germany

⁴⁴ Institut für Kern- und Teilchenphysik, Technische Universität Dresden, Dresden, Germany

⁴⁵ Department of Physics, Duke University, Durham NC, United States of America

⁴⁶ SUPA - School of Physics and Astronomy, University of Edinburgh, Edinburgh, United Kingdom

⁴⁷ INFN Laboratori Nazionali di Frascati, Frascati, Italy

⁴⁸ Fakultät für Mathematik und Physik, Albert-Ludwigs-Universität, Freiburg, Germany

⁴⁹ Section de Physique, Université de Genève, Geneva, Switzerland

⁵⁰ ^(a) INFN Sezione di Genova; ^(b) Dipartimento di Fisica, Università di Genova, Genova, Italy

⁵¹ ^(a) E. Andronikashvili Institute of Physics, Iv. Javakishvili Tbilisi State University, Tbilisi; ^(b) High Energy Physics Institute, Tbilisi State University, Tbilisi, Georgia

⁵² II Physikalisches Institut, Justus-Liebig-Universität Giessen, Giessen, Germany

⁵³ SUPA - School of Physics and Astronomy, University of Glasgow, Glasgow, United Kingdom

⁵⁴ II Physikalisches Institut, Georg-August-Universität, Göttingen, Germany

⁵⁵ Laboratoire de Physique Subatomique et de Cosmologie, Université Grenoble-Alpes, CNRS/IN2P3, Grenoble, France

⁵⁶ Department of Physics, Hampton University, Hampton VA, United States of America

⁵⁷ Laboratory for Particle Physics and Cosmology, Harvard University, Cambridge MA, United States of America

⁵⁸ ^(a) Kirchhoff-Institut für Physik, Ruprecht-Karls-Universität Heidelberg, Heidelberg; ^(b) Physikalisches Institut, Ruprecht-Karls-Universität Heidelberg, Heidelberg; ^(c) ZITI Institut für technische Informatik, Ruprecht-Karls-Universität Heidelberg, Mannheim, Germany

⁵⁹ Faculty of Applied Information Science, Hiroshima Institute of Technology, Hiroshima, Japan

⁶⁰ Department of Physics, Indiana University, Bloomington IN, United States of America

⁶¹ Institut für Astro- und Teilchenphysik, Leopold-Franzens-Universität, Innsbruck, Austria

⁶² University of Iowa, Iowa City IA, United States of America

⁶³ Department of Physics and Astronomy, Iowa State University, Ames IA, United States of America

⁶⁴ Joint Institute for Nuclear Research, JINR Dubna, Dubna, Russia

⁶⁵ KEK, High Energy Accelerator Research Organization, Tsukuba, Japan

⁶⁶ Graduate School of Science, Kobe University, Kobe, Japan

⁶⁷ Faculty of Science, Kyoto University, Kyoto, Japan

⁶⁸ Kyoto University of Education, Kyoto, Japan

⁶⁹ Department of Physics, Kyushu University, Fukuoka, Japan

⁷⁰ Instituto de Física La Plata, Universidad Nacional de La Plata and CONICET, La Plata, Argentina

⁷¹ Physics Department, Lancaster University, Lancaster, United Kingdom

⁷² ^(a) INFN Sezione di Lecce; ^(b) Dipartimento di Matematica e Fisica, Università del Salento, Lecce, Italy

⁷³ Oliver Lodge Laboratory, University of Liverpool, Liverpool, United Kingdom

- ⁷⁴ Department of Physics, Jožef Stefan Institute and University of Ljubljana, Ljubljana, Slovenia
- ⁷⁵ School of Physics and Astronomy, Queen Mary University of London, London, United Kingdom
- ⁷⁶ Department of Physics, Royal Holloway University of London, Surrey, United Kingdom
- ⁷⁷ Department of Physics and Astronomy, University College London, London, United Kingdom
- ⁷⁸ Louisiana Tech University, Ruston LA, United States of America
- ⁷⁹ Laboratoire de Physique Nucléaire et de Hautes Energies, UPMC and Université Paris-Diderot and CNRS/IN2P3, Paris, France
- ⁸⁰ Fysiska institutionen, Lunds universitet, Lund, Sweden
- ⁸¹ Departamento de Física Teórica C-15, Universidad Autónoma de Madrid, Madrid, Spain
- ⁸² Institut für Physik, Universität Mainz, Mainz, Germany
- ⁸³ School of Physics and Astronomy, University of Manchester, Manchester, United Kingdom
- ⁸⁴ CPPM, Aix-Marseille Université and CNRS/IN2P3, Marseille, France
- ⁸⁵ Department of Physics, University of Massachusetts, Amherst MA, United States of America
- ⁸⁶ Department of Physics, McGill University, Montreal QC, Canada
- ⁸⁷ School of Physics, University of Melbourne, Victoria, Australia
- ⁸⁸ Department of Physics, The University of Michigan, Ann Arbor MI, United States of America
- ⁸⁹ Department of Physics and Astronomy, Michigan State University, East Lansing MI, United States of America
- ⁹⁰ ^(a) INFN Sezione di Milano; ^(b) Dipartimento di Fisica, Università di Milano, Milano, Italy
- ⁹¹ B.I. Stepanov Institute of Physics, National Academy of Sciences of Belarus, Minsk, Republic of Belarus
- ⁹² National Scientific and Educational Centre for Particle and High Energy Physics, Minsk, Republic of Belarus
- ⁹³ Department of Physics, Massachusetts Institute of Technology, Cambridge MA, United States of America
- ⁹⁴ Group of Particle Physics, University of Montreal, Montreal QC, Canada
- ⁹⁵ P.N. Lebedev Institute of Physics, Academy of Sciences, Moscow, Russia
- ⁹⁶ Institute for Theoretical and Experimental Physics (ITEP), Moscow, Russia
- ⁹⁷ Moscow Engineering and Physics Institute (MEPhI), Moscow, Russia
- ⁹⁸ D.V.Skobel'syn Institute of Nuclear Physics, M.V.Lomonosov Moscow State University, Moscow, Russia
- ⁹⁹ Fakultät für Physik, Ludwig-Maximilians-Universität München, München, Germany
- ¹⁰⁰ Max-Planck-Institut für Physik (Werner-Heisenberg-Institut), München, Germany
- ¹⁰¹ Nagasaki Institute of Applied Science, Nagasaki, Japan
- ¹⁰² Graduate School of Science and Kobayashi-Maskawa Institute, Nagoya University, Nagoya, Japan
- ¹⁰³ ^(a) INFN Sezione di Napoli; ^(b) Dipartimento di Fisica, Università di Napoli, Napoli, Italy
- ¹⁰⁴ Department of Physics and Astronomy, University of New Mexico, Albuquerque NM, United States of America
- ¹⁰⁵ Institute for Mathematics, Astrophysics and Particle Physics, Radboud University Nijmegen/Nikhef, Nijmegen, Netherlands
- ¹⁰⁶ Nikhef National Institute for Subatomic Physics and University of Amsterdam, Amsterdam, Netherlands
- ¹⁰⁷ Department of Physics, Northern Illinois University, DeKalb IL, United States of America
- ¹⁰⁸ Budker Institute of Nuclear Physics, SB RAS, Novosibirsk, Russia
- ¹⁰⁹ Department of Physics, New York University, New York NY, United States of America
- ¹¹⁰ Ohio State University, Columbus OH, United States of America
- ¹¹¹ Faculty of Science, Okayama University, Okayama, Japan
- ¹¹² Homer L. Dodge Department of Physics and Astronomy, University of Oklahoma, Norman OK, United States of America
- ¹¹³ Department of Physics, Oklahoma State University, Stillwater OK, United States of America
- ¹¹⁴ Palacký University, RCPTM, Olomouc, Czech Republic
- ¹¹⁵ Center for High Energy Physics, University of Oregon, Eugene OR, United States of America
- ¹¹⁶ LAL, Université Paris-Sud and CNRS/IN2P3, Orsay, France
- ¹¹⁷ Graduate School of Science, Osaka University, Osaka, Japan
- ¹¹⁸ Department of Physics, University of Oslo, Oslo, Norway
- ¹¹⁹ Department of Physics, Oxford University, Oxford, United Kingdom
- ¹²⁰ ^(a) INFN Sezione di Pavia; ^(b) Dipartimento di Fisica, Università di Pavia, Pavia, Italy
- ¹²¹ Department of Physics, University of Pennsylvania, Philadelphia PA, United States of America
- ¹²² Petersburg Nuclear Physics Institute, Gatchina, Russia
- ¹²³ ^(a) INFN Sezione di Pisa; ^(b) Dipartimento di Fisica E. Fermi, Università di Pisa, Pisa, Italy
- ¹²⁴ Department of Physics and Astronomy, University of Pittsburgh, Pittsburgh PA, United States of America
- ¹²⁵ ^(a) Laboratório de Instrumentação e Física Experimental de Partículas - LIP, Lisboa; ^(b) Faculdade de Ciências, Universidade de Lisboa, Lisboa; ^(c) Department of Physics, University of Coimbra, Coimbra; ^(d) Centro de Física Nuclear da Universidade de Lisboa, Lisboa; ^(e) Departamento de Física, Universidade do Minho, Braga; ^(f) Departamento de Física Teórica y del Cosmos and CAFPE, Universidad de Granada, Granada (Spain); ^(g) Dep Física and CEFITEC of Faculdade de Ciências e Tecnologia, Universidade Nova de Lisboa, Caparica, Portugal
- ¹²⁶ Institute of Physics, Academy of Sciences of the Czech Republic, Praha, Czech Republic

- 127 Czech Technical University in Prague, Praha, Czech Republic
- 128 Faculty of Mathematics and Physics, Charles University in Prague, Praha, Czech Republic
- 129 State Research Center Institute for High Energy Physics, Protvino, Russia
- 130 Particle Physics Department, Rutherford Appleton Laboratory, Didcot, United Kingdom
- 131 Physics Department, University of Regina, Regina SK, Canada
- 132 Ritsumeikan University, Kusatsu, Shiga, Japan
- 133 ^(a) INFN Sezione di Roma; ^(b) Dipartimento di Fisica, Sapienza Università di Roma, Roma, Italy
- 134 ^(a) INFN Sezione di Roma Tor Vergata; ^(b) Dipartimento di Fisica, Università di Roma Tor Vergata, Roma, Italy
- 135 ^(a) INFN Sezione di Roma Tre; ^(b) Dipartimento di Matematica e Fisica, Università Roma Tre, Roma, Italy
- 136 ^(a) Faculté des Sciences Ain Chock, Réseau Universitaire de Physique des Hautes Energies - Université Hassan II, Casablanca; ^(b) Centre National de l'Énergie des Sciences Techniques Nucleaires, Rabat; ^(c) Faculté des Sciences Semlalia, Université Cadi Ayyad, LPHEA-Marrakech; ^(d) Faculté des Sciences, Université Mohamed Premier and LTPM, Oujda; ^(e) Faculté des sciences, Université Mohammed V-Agdal, Rabat, Morocco
- 137 DSM/IRFU (Institut de Recherches sur les Lois Fondamentales de l'Univers), CEA Saclay (Commissariat à l'Énergie Atomique et aux Énergies Alternatives), Gif-sur-Yvette, France
- 138 Santa Cruz Institute for Particle Physics, University of California Santa Cruz, Santa Cruz CA, United States of America
- 139 Department of Physics, University of Washington, Seattle WA, United States of America
- 140 Department of Physics and Astronomy, University of Sheffield, Sheffield, United Kingdom
- 141 Department of Physics, Shinshu University, Nagano, Japan
- 142 Fachbereich Physik, Universität Siegen, Siegen, Germany
- 143 Department of Physics, Simon Fraser University, Burnaby BC, Canada
- 144 SLAC National Accelerator Laboratory, Stanford CA, United States of America
- 145 ^(a) Faculty of Mathematics, Physics & Informatics, Comenius University, Bratislava; ^(b) Department of Subnuclear Physics, Institute of Experimental Physics of the Slovak Academy of Sciences, Kosice, Slovak Republic
- 146 ^(a) Department of Physics, University of Cape Town, Cape Town; ^(b) Department of Physics, University of Johannesburg, Johannesburg; ^(c) School of Physics, University of the Witwatersrand, Johannesburg, South Africa
- 147 ^(a) Department of Physics, Stockholm University; ^(b) The Oskar Klein Centre, Stockholm, Sweden
- 148 Physics Department, Royal Institute of Technology, Stockholm, Sweden
- 149 Departments of Physics & Astronomy and Chemistry, Stony Brook University, Stony Brook NY, United States of America
- 150 Department of Physics and Astronomy, University of Sussex, Brighton, United Kingdom
- 151 School of Physics, University of Sydney, Sydney, Australia
- 152 Institute of Physics, Academia Sinica, Taipei, Taiwan
- 153 Department of Physics, Technion: Israel Institute of Technology, Haifa, Israel
- 154 Raymond and Beverly Sackler School of Physics and Astronomy, Tel Aviv University, Tel Aviv, Israel
- 155 Department of Physics, Aristotle University of Thessaloniki, Thessaloniki, Greece
- 156 International Center for Elementary Particle Physics and Department of Physics, The University of Tokyo, Tokyo, Japan
- 157 Graduate School of Science and Technology, Tokyo Metropolitan University, Tokyo, Japan
- 158 Department of Physics, Tokyo Institute of Technology, Tokyo, Japan
- 159 Department of Physics, University of Toronto, Toronto ON, Canada
- 160 ^(a) TRIUMF, Vancouver BC; ^(b) Department of Physics and Astronomy, York University, Toronto ON, Canada
- 161 Faculty of Pure and Applied Sciences, University of Tsukuba, Tsukuba, Japan
- 162 Department of Physics and Astronomy, Tufts University, Medford MA, United States of America
- 163 Centro de Investigaciones, Universidad Antonio Narino, Bogota, Colombia
- 164 Department of Physics and Astronomy, University of California Irvine, Irvine CA, United States of America
- 165 ^(a) INFN Gruppo Collegato di Udine, Sezione di Trieste, Udine; ^(b) ICTP, Trieste; ^(c) Dipartimento di Chimica, Fisica e Ambiente, Università di Udine, Udine, Italy
- 166 Department of Physics, University of Illinois, Urbana IL, United States of America
- 167 Department of Physics and Astronomy, University of Uppsala, Uppsala, Sweden
- 168 Instituto de Física Corpuscular (IFIC) and Departamento de Física Atómica, Molecular y Nuclear and Departamento de Ingeniería Electrónica and Instituto de Microelectrónica de Barcelona (IMB-CNM), University of Valencia and CSIC, Valencia, Spain
- 169 Department of Physics, University of British Columbia, Vancouver BC, Canada
- 170 Department of Physics and Astronomy, University of Victoria, Victoria BC, Canada
- 171 Department of Physics, University of Warwick, Coventry, United Kingdom
- 172 Waseda University, Tokyo, Japan
- 173 Department of Particle Physics, The Weizmann Institute of Science, Rehovot, Israel
- 174 Department of Physics, University of Wisconsin, Madison WI, United States of America

- ¹⁷⁵ Fakultät für Physik und Astronomie, Julius-Maximilians-Universität, Würzburg, Germany
- ¹⁷⁶ Fachbereich C Physik, Bergische Universität Wuppertal, Wuppertal, Germany
- ¹⁷⁷ Department of Physics, Yale University, New Haven CT, United States of America
- ¹⁷⁸ Yerevan Physics Institute, Yerevan, Armenia
- ¹⁷⁹ Centre de Calcul de l'Institut National de Physique Nucléaire et de Physique des Particules (IN2P3), Villeurbanne, France
- ^a Also at Department of Physics, King's College London, London, United Kingdom
- ^b Also at Institute of Physics, Azerbaijan Academy of Sciences, Baku, Azerbaijan
- ^c Also at Particle Physics Department, Rutherford Appleton Laboratory, Didcot, United Kingdom
- ^d Also at TRIUMF, Vancouver BC, Canada
- ^e Also at Department of Physics, California State University, Fresno CA, United States of America
- ^f Also at CPPM, Aix-Marseille Université and CNRS/IN2P3, Marseille, France
- ^g Also at Università di Napoli Parthenope, Napoli, Italy
- ^h Also at Institute of Particle Physics (IPP), Canada
- ⁱ Also at Department of Physics, St. Petersburg State Polytechnical University, St. Petersburg, Russia
- ^j Also at Department of Financial and Management Engineering, University of the Aegean, Chios, Greece
- ^k Also at Louisiana Tech University, Ruston LA, United States of America
- ^l Also at Institutio Catalana de Recerca i Estudis Avancats, ICREA, Barcelona, Spain
- ^m Also at Department of Physics, The University of Texas at Austin, Austin TX, United States of America
- ⁿ Also at Institute of Theoretical Physics, Iliia State University, Tbilisi, Georgia
- ^o Also at CERN, Geneva, Switzerland
- ^p Also at Ochadai Academic Production, Ochanomizu University, Tokyo, Japan
- ^q Also at Manhattan College, New York NY, United States of America
- ^r Also at Novosibirsk State University, Novosibirsk, Russia
- ^s Also at Institute of Physics, Academia Sinica, Taipei, Taiwan
- ^t Also at LAL, Université Paris-Sud and CNRS/IN2P3, Orsay, France
- ^u Also at Academia Sinica Grid Computing, Institute of Physics, Academia Sinica, Taipei, Taiwan
- ^v Also at Laboratoire de Physique Nucléaire et de Hautes Energies, UPMC and Université Paris-Diderot and CNRS/IN2P3, Paris, France
- ^w Also at School of Physical Sciences, National Institute of Science Education and Research, Bhubaneswar, India
- ^x Also at Dipartimento di Fisica, Sapienza Università di Roma, Roma, Italy
- ^y Also at Moscow Institute of Physics and Technology State University, Dolgoprudny, Russia
- ^z Also at Section de Physique, Université de Genève, Geneva, Switzerland
- ^{aa} Also at International School for Advanced Studies (SISSA), Trieste, Italy
- ^{ab} Also at Department of Physics and Astronomy, University of South Carolina, Columbia SC, United States of America
- ^{ac} Also at School of Physics and Engineering, Sun Yat-sen University, Guangzhou, China
- ^{ad} Also at Faculty of Physics, M.V.Lomonosov Moscow State University, Moscow, Russia
- ^{ae} Also at Moscow Engineering and Physics Institute (MEPhI), Moscow, Russia
- ^{af} Also at Institute for Particle and Nuclear Physics, Wigner Research Centre for Physics, Budapest, Hungary
- ^{ag} Also at Department of Physics, Oxford University, Oxford, United Kingdom
- ^{ah} Also at Department of Physics, Nanjing University, Jiangsu, China
- ^{ai} Also at Institut für Experimentalphysik, Universität Hamburg, Hamburg, Germany
- ^{aj} Also at Department of Physics, The University of Michigan, Ann Arbor MI, United States of America
- ^{ak} Also at Discipline of Physics, University of KwaZulu-Natal, Durban, South Africa
- * Deceased